Oxygen Electrodes

Semiconductor Anodes

Showcasing research from the Ertl Center for Electrochemistry and Catalysis, RISE of Prof. Dr Jaeyoung Lee and Mr Joey D. Ocon at Gwangju Institute of Science and Technology, South Korea

Title: Quasi-perpetual discharge behaviour in p-type Ge–air batteries

Metal–air batteries are extremely attractive energy storage and conversion systems due to their high energy and power densities, safer chemistries, and economic viability. A new type of metal–air batteries, semiconductor–air batteries running on Si or Ge anodes offer very high energy densities relative to conventional anodes. P-type Ge–air batteries exhibit an unprecedented full discharge capacity of 88% of its theoretical capacity. In complement with inexpensive iron-triad element-based air electrodes (Fe, Co, and Ni), semiconductor–air batteries in alkaline media could supply power in specific applications in the future.

As featured in:
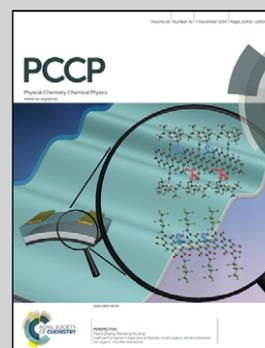
www.rsc.org/pccp

ROYAL SOCIETY OF CHEMISTRY

Quasi-perpetual discharge behaviour in p-type Ge–air batteries†

Joey D. Ocon,[a] Jin Won Kim,[a] Graniel Harne A. Abrenica,[a] Jae Kwang Lee[b] and Jaeyoung Lee*[ab]

Metal–air batteries continue to become attractive energy storage and conversion systems due to their high energy and power densities, safer chemistries, and economic viability. Semiconductor–air batteries – a term we first define here as metal–air batteries that use semiconductor anodes such as silicon (Si) and germanium (Ge) – have been introduced in recent years as new high-energy battery chemistries. In this paper, we describe the excellent doping-dependent discharge kinetics of p-type Ge anodes in a semiconductor–air cell employing a gelled KOH electrolyte. Owing to its Fermi level, n-type Ge is expected to have lower redox potential and better electronic conductivity, which could potentially lead to a higher operating voltage and better discharge kinetics. Nonetheless, discharge measurements demonstrated that this prediction is only valid at the low current regime and breaks down at the high current density region. The p-type Ge behaves extremely better at elevated currents, evident from the higher voltage, more power available, and larger practical energy density from a very long discharge time, possibly arising from the high overpotential for surface passivation. A primary semiconductor–air battery, powered by a flat p-type Ge as a multi-electron anode, exhibited an unprecedented full discharge capacity of 1302.5 mA h g_{Ge}^{-1} (88% anode utilization efficiency), the highest among semiconductor–air cells, notably better than new metal–air cells with three-dimensional and nanostructured anodes, and at least two folds higher than commercial Zn–air and Al–air cells. We therefore suggest that this study be extended to doped-Si anodes, in order to pave the way for a deeper understanding on the discharge phenomena in alkaline metal–air conversion cells with semiconductor anodes for specific niche applications in the future.

1. Introduction

Metal–air batteries are ideal high-energy storage and conversion systems for a wide array of applications due to their low overall weights and straightforward designs, which can lead to significant cost savings.[1–4] This arises from the unique feature of metal–air batteries, when compared with other batteries, such that one of the electroactive materials (*i.e.* oxygen) does not need to be stored within the system. With abundant supply of oxygen in the air, metal–air batteries have extremely higher theoretical energy densities than their traditional aqueous and lithium-ion counterparts.[5] Furthermore, metal–air batteries, particularly those with aqueous chemistries, are generally classified as safe and inexpensive, fire-prone alternatives to hazardous lithium batteries. Different metals (*e.g.* zinc (Zn),[6] aluminum (Al),[7] and lithium (Li)[8]) and metal-based compounds (*e.g.* borides,[9] silicides,[10] and phosphides[11]) have been studied as anode materials for metal–air batteries. Although the chemistries of these metal–air batteries offer high-energy capacities, the anode utilization efficiency in most of these cells (*i.e.* Zn–air battery) are highly limited to only 60% below the theoretical capacity.[12,13] Immediate passivation of the metal anodes (*e.g.* Al, Mg) during discharge severely cuts the available energy and makes the rest of the anode unusable. It is therefore of great technological importance to improve the discharge behaviour of these anodes, or alternatively, to find new chemistries with better discharge kinetics than the previously reported anodes.

Of late, semiconductor–air batteries, a term we first define here as metal–air batteries that use a semiconductor anode such as silicon (Si, 3822 mA h g_{Si}^{-1})[14–17] and germanium (Ge, 1477 mA h g_{Ge}^{-1}),[18]

[a] *Electrochemical Reaction and Technology Laboratory (ERTL), School of Environmental Science and Engineering, Gwangju Institute of Science and Technology, Gwangju 500-712, South Korea. E-mail: jaeyoung@gist.ac.kr*

[b] *ERTL Center for Electrochemistry and Catalysis, Research Institute for Solar and Sustainable Energies (RISE), Gwangju Institute of Science and Technology, Gwangju 500-712, South Korea*

† Electronic supplementary information (ESI) available: Photograph of the semiconductor–air cell, dynamic step discharge response of heavily doped flat Si anodes at various current drains, SEM images and X-ray diffractograms of the electrodes before and after full discharge, Computed Ge mass loss during long-term discharge of p-type Ge due to self-discharge, XP spectra of the electrodes before and after full discharge, comparison of practical energy density and anode utilization efficiency of different metal–air batteries, and images of different gelled KOH electrolytes with varying gelling agent amounts. See DOI: 10.1039/c4cp02134g

This journal is © the Owner Societies 2014

*Phys. Chem. Chem. Phys.,* 2014, **16**, 22487–22494 | 22487

have been introduced as high capacity anode materials. Of the semiconductor–air batteries based on pure Si as the anode, two types of electrolytes have been used: an aqueous alkaline electrolyte and a room temperature ionic liquid (RTIL) electrolyte. Si–air batteries, using an RTIL electrolyte, were predominantly studied using n-type Si wafers because they can lead to a higher operating voltage, despite higher corrosion rates.[14–16] Although various p-type and n-type doped Si wafers, with different doping levels and crystal orientations, have been initially screened, only polarization voltammograms were used to evaluate the anodes, leading to the conclusion that n-type Si is the best candidate. On the other hand, the Si–air battery with an alkaline electrolyte utilized only porous n-type Si wafers of various doping levels.[17] They reported a discharge capacity, however, of only $\sim$30% of the theoretical anode capacity, and no full discharge curves were obtained. Hence, the extent of the effect of the doping type and level on the discharge kinetics in semiconductor anodes has neither been discovered nor understood yet.

In our previous study, we first reported the successful operation of a novel semiconductor–air battery, running on a p-type Ge (0.019–0.024 Ω cm) anode in an alkaline electrolyte. The formation of ordered hierarchical porous structures, *via* controlled etching, improved the energy capacity of the Ge–air cell, showing a stable long-term discharge profile.[18] Our discussion, however, was limited only to the formation of the nanoporous structure and the surface oxide coverage after etching and its effect on the discharge kinetics of Ge–air cell. Nevertheless, earlier studies and our results suggest that doped semiconductors (Ge and Si) are indeed viable high energy density anodes for metal–air energy conversion cells, in addition to being suitable candidates for next generation lithium ion batteries.[19]

In this paper, we explore the effect of the doping type and level on the discharge kinetics of Ge anodes in a semiconductor–air cell. By studying the discharge of the semiconductor–air cells with various anodes, we demonstrate the unexpected excellent performance of p-type Ge in comparison with other Ge anodes. In addition, our results indicate that the semiconductor–air battery, based on a flat Ge anode, offers as high as 1302.5 mA h g_{Ge}^{-1} of practical energy density, which is two and three times higher than that of commercial Zn–air and Al–air batteries, respectively.

2. Results and discussion

Following the design of a semiconductor–air cell we have previously used, we modified the cell to decrease the gap between the anode and cathode. Semiconductor anodes were tested using the simple device architecture, consisting of Ge wafer as the anode, a gelled KOH as the electrolyte, and 46.7 wt% platinum on carbon (Pt/C) as the cathode (Fig. S1, ESI†). Pt/C was used as the oxygen reduction reaction (ORR) catalyst in order to make sure that the performance difference will be coming solely from the different anodes only. Meanwhile, the gelled KOH
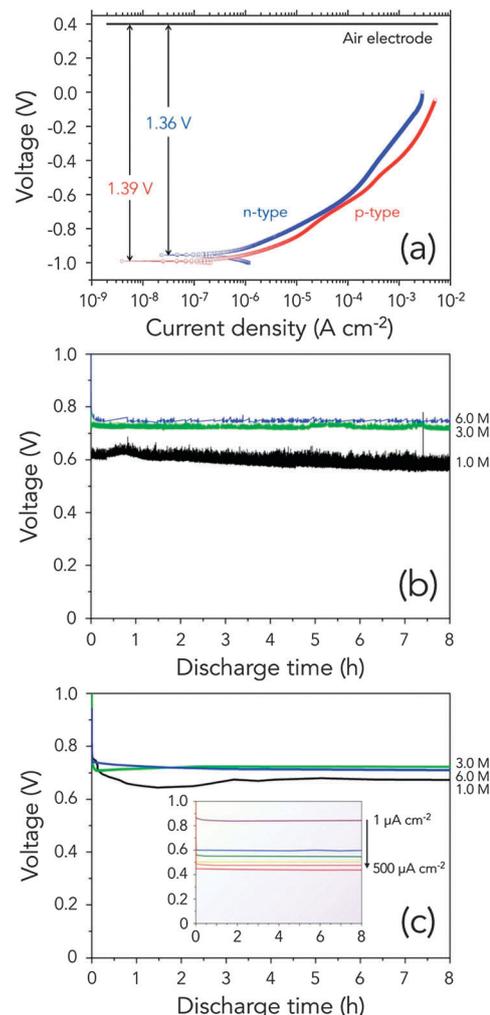
Fig. 1 (a) Potentiodynamic curves of n-type Ge and p-type Ge in 6.0 M KOH electrolyte at a scan rate of 5 mV s^{-1}. Galvanostatic discharge curves of a Ge–air battery using n-type Ge and p-type Ge in a gelled electrolyte at various KOH concentrations and discharge current densities: (b) n-type Ge–air cell operating at a discharge current density of 10 μA cm^{-2} at various KOH concentrations and (c) p-type Ge–air cell operating at a discharge current density of 10 μA cm^{-2} at various KOH concentrations. The inset shows the p-type Ge–air cell in 6.0 M gelled KOH electrolyte at various discharge current densities, with the decreasing operating voltages corresponding to the following current densities: 1, 50, 100, 200, 300, and 500 μA cm^{-2}. Both n-type Ge and p-type Ge can be considered as heavily doped Ge wafers, with the following average resistivities: n-type Ge (0.007 Ω cm), p-type Ge (0.0145 Ω cm).

electrolyte was prepared by adding carboxymethyl cellulose (CMC) into the KOH solution. Gelling agents have been widely used to enhance the electrochemical performance of zinc–air cells and prevent leakage of the KOH electrolyte.[20] Highly concentrated KOH solutions were used in order to limit the ohmic polarization and to make sure that the discharge products, mainly Ge(OH)$_2$, are easily dissolved in the electrolyte.

Fig. 1a shows the potentiodynamic curves comparing n-type Ge and p-type Ge. As seen in the curves, the expected cell voltage of the two anodes at low current drains does not differ much, contrary to what was observed in Si–air batteries with the
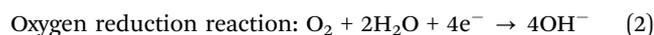
RTIL electrolyte, where n-type Si exhibited a relatively high operating potential than p-type Si at the low current regime.[15] In fact, the two curves are close to one another throughout the entire range of current densities, implying that the discharge kinetics could not be too different. The anodic dissolution current densities rapidly increase (−1.0 V to −0.7 V) at first and then flattened at a more positive potential. Both types of doped Ge, however, have relatively large oxidation overpotentials at the high current density region, which can lead to a lower operating potential.

As a preliminary test of Ge–air cell performance, Ge–air cells were constructed using different gelled KOH concentrations (1.0 M, 3.0 M, and 6.0 M) and discharged at different current densities (1–500 μA cm^{-2}). The typical discharge plots of the n-type Ge–air cell at different KOH concentrations, measured under constant current mode of operation, are shown in Fig. 1b. As the KOH concentration increases, n-type Ge operates at higher potentials. Increasing the KOH concentration, however, has a drawback since it can lead to elevated corrosion rates in the anode, decreasing the energy available for the cell's operation. Fluctuation in the operating potential, which increases as the electrolyte concentration is lowered, has been observed during discharge, indicating a possible instability in the anode. This behaviour has been likewise observed in alkaline Si–air batteries that run on n-type Si anodes.[17]

In contrast, p-type Ge–air cells operated at the highest potential when 3.0 M gelled KOH electrolyte (Fig. 1c) was used. It is good to also note that the voltage fluctuation observed in n-type Ge is absent in p-type Ge, as shown in the very flat discharge profiles. In order to confirm the flat discharge profiles of p-type Ge, we tested the discharge behaviour of p-type Ge at various current drains. The inset of Fig. 1c demonstrates the flat discharge profiles of p-type Ge–air cells, operating at higher voltage when decreasing the amount of current drawn. In fuel cell operation, which is somehow similar to how semiconductor–air cells work, the drop in potential with increasing current can be attributed to the increase in the internal resistance of the cell, especially in between the electrode/electrolyte interfaces.[21]

To fully explain the discharge behaviour of the different Ge anodes, it is important to revisit the three main reactions during the Ge–air cell discharge in an alkaline electrolyte, as written below. During discharge, Ge is oxidized to produce four electrons, which are accepted by the cathode to reduce an oxygen molecule into hydroxide ions. Slow dissolution of the Ge(OH)$_4$ into the electrolyte, in combination with fast anode oxidation kinetics, results in the passivation of the anode.[18]

$$\text{Anode discharge: Ge} + 4\text{OH}^- \rightarrow \text{Ge(OH)}_4 + 4e^- \quad (1)$$

$$\text{Oxygen reduction reaction: O}_2 + 2\text{H}_2\text{O} + 4e^- \rightarrow 4\text{OH}^- \quad (2)$$

$$\text{Surface passivation: Ge(OH)}_4 \rightarrow \text{GeO}_2 + 2\text{H}_2\text{O} \quad (3)$$

The observed fluctuations in the discharge of n-type Ge can be assumed to arise from the interplay between the dissolution of Ge(OH)$_4$ into the electrolyte and the dehydration reaction that passivates the Ge surface. The increase in the amplitude of the fluctuations with decreasing KOH concentration provides ample evidence to this hypothesis. At low KOH concentrations, the formation rate of Ge(OH)$_2$ exceeds its dissolution rate, decreasing the cell voltage due to surface passivation. Surface passivation, however, has not yet reached a critical level and the oxide is intermittently removed with the continuous discharge, causing an increase in the operating voltage, and the cycle goes on. In contrast, p-type Ge has a very flat discharge profile, which denotes that the surface passivation proceeds at a slower rate, possibly resulting from the higher passivation overpotential of p-type Ge than that of n-type Ge. These results indicate that the electrochemical activity of p-type Ge is significantly more reliable than that of n-type Ge, even if they have comparable dopant concentrations.

In order to account for the self-discharge of the Ge–air cells at open circuit potential (OCP), we measured the corrosion rates of both heavily doped n-type Ge and p-type Ge in the 6.0 M gelled KOH electrolyte by performing linear polarization experiments in the range of ±20 mV relative to the OCP. As seen in Fig. 2a, p-type Ge corrodes faster than n-type Ge, contrary to the trend found in Si anodes in the RTIL electrolyte, where n-type Si generally shows higher corrosion currents than p-type Si. The low overpotential for passivation in n-type Ge might explain this extremely low corrosion rate. Once passivated, electrolyte ions can no longer attack the metallic Ge on the surface. However, although p-type Ge has a relatively fast corrosion kinetics than n-type in the cell environment, the measured corrosion rates are not that high and are comparable to that of Si in the RTIL electrolyte,[15] and even in highly resistive metals in extreme environments.[22]

Fig. 2b shows the Nyquist plots of n-type Ge and p-type Ge in the semiconductor–air cell with the gelled KOH electrolyte at OCP before any discharge experiment. As shown in the impedance spectra, p-type Ge and n-type Ge behave similarly, but n-type Ge has a lower value of the real axis intercept. At the high frequency region, the intercept with the real axis corresponds to the equivalent series resistance of the cell. As shown in the inset of Fig. 2b, however, p-type Ge (6.3 Ω) has a relatively low electrical resistance than n-type Ge (49.8 Ω), when the impedance was measured after the cell was discharged at 50 μA cm^{-2} for 8 h. This might have arisen from the higher rate of passivation on the surface of the n-type Ge anode, increasing the resistance of the cell.

The operating voltage of metal–air cells can be seen as a measure of the efficiency of the cells, since maintaining a high battery voltage – even at higher current loads – is critical to the successful implementation of the battery technology. From the results above, the difference in discharge kinetics shown in Fig. 1 is not much evident. Hence, we measured the potential response of various Ge anodes with an incremental increase in current density drawn from the cell, in order to generate the current–potential (J–V) and the power curves of the Ge–air cell with various anodes. The current of the Ge–air cell was held fixed in time and the pseudo-steady state value of the cell voltage was recorded after a long equilibration time ($\sim$10 min).
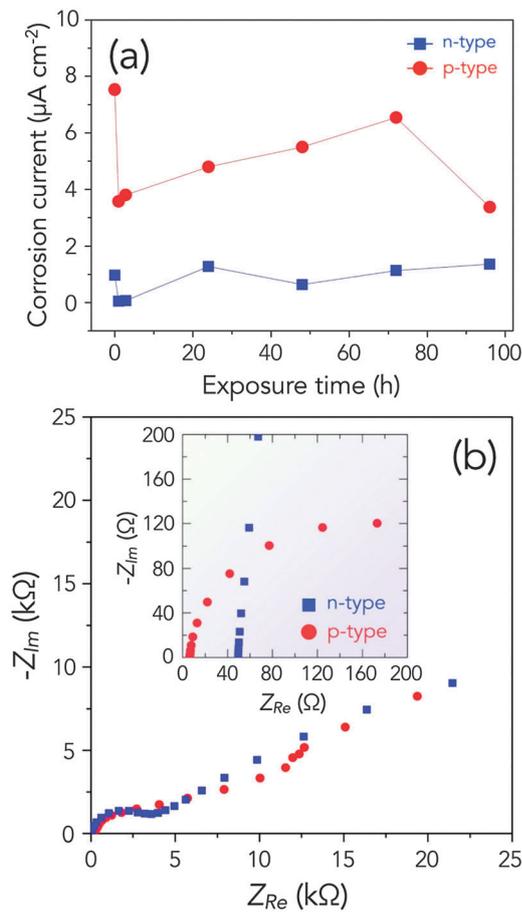
Fig. 2 (a) Corrosion rates of the n-type Ge and p-type Ge (both heavily doped) in the semiconductor–air cell as a function of the exposure time in the 6.0 M gelled KOH electrolyte at open circuit potential. (b) Nyquist plots for n-type Ge and p-type Ge in the semiconductor–air cell with a 6.0 M gelled KOH electrolyte and Pt/C cathode. The inset shows the behaviour of the Ge anodes at the high frequency region after discharging for 8 h at a current density of 50 $\mu A\ cm^{-2}$.
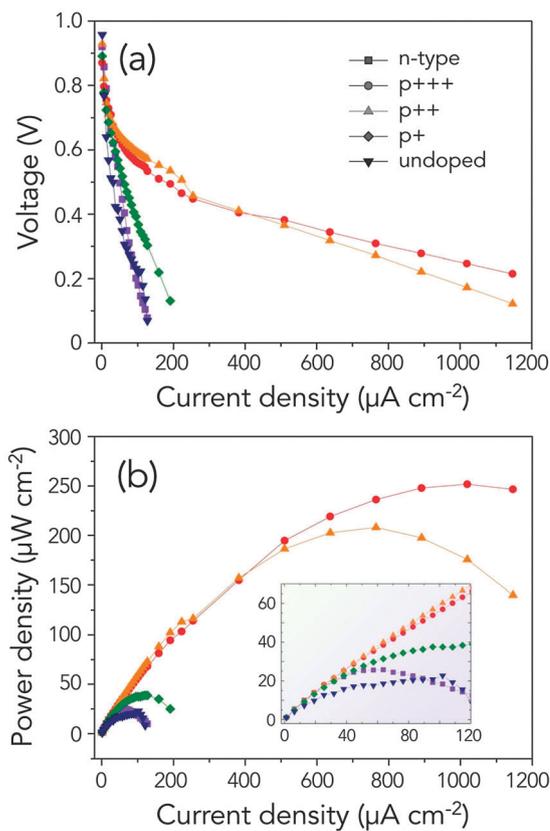
Fig. 3 (a) Current–potential (J–V) curves and (b) power curves for Ge–air cells operated using different anode types: heavily doped n-type Ge, undoped Ge, and p-type Ge with various doping levels: heavily doped (p+++), medium doped (p++), and lightly doped (p+). P-doped Ge anodes were doped with gallium (Ga) while the heavily doped n-type Ge was doped with antimony (Sb). The inset figure in (b) displays the power behaviour at the low current region. All Ge–air cells were operated using a 6.0 M gelled KOH electrolyte under ambient conditions. Furthermore, the cells were aged for 3 h to ensure that the electrodes are already in full contact with the gelled electrolyte.

As seen in Fig. 3, various Ge wafers revealed different behaviours as semiconductor–air anodes. For instance, n-type Ge has a slightly better discharge kinetics over any p-type Ge at the low current regime ($< 20\ \mu A\ cm^{-2}$). There is, however, a large drop in operating potential beyond this region, indicating a strong passivation behaviour in n-type Ge, whereas, p-type Ge displays a gradual decrease in potential with increasing current. This is contrary to the small variation in electrochemical behaviour of n-type Ge and p-type Ge, as observed in the potentiodynamic curves shown in Fig. 1a. Unexpectedly, n-type Ge behaves similarly to the undoped Ge, raising an important question as to why, despite having good electrical conductivity (almost five orders of magnitude) and electronegativity (high dopant concentrations), the discharge kinetics of n-type Ge is much poorer than expected.

In contrast, as seen in the representative J–V plots, p-type Ge anodes have increasingly improved discharge kinetics as the doping degree increases. This is manifested by the higher operating voltage and the more gradual decrease of potential

at high current densities. Unlike in fuel cell operation, where the voltage quickly drops due to mass diffusion limitation and ohmic resistance at higher currents, we assume that the decrease in operating voltage in semiconductor anodes can be largely explained by the faster passivation of the anode's surface. As shown in the power curves in Fig. 3b, the heavily doped p-type Ge (p+++) exhibits the best discharge kinetics, especially at higher currents. At the low current regime (inset of Fig. 3b), however, medium doped p-type Ge (p++) demonstrates the highest power density.

Table 1 summarizes the doping information and electrochemical discharge kinetics of undoped and doped semiconductor anodes. The resistivity data were gathered from the manufacturer of semiconductor wafers, while the carrier concentration can be derived from the resistivity *versus* impurity concentration plot.[23] For instance, for the same dopant concentration, n-type Ge has a relatively lower resistivity than p-type Ge. In order to facilitate an easier comparison of the discharge kinetics of semiconductor anodes, heavily doped

22490 | *Phys. Chem. Chem. Phys.*, 2014, **16**, 22487–22494

This journal is © the Owner Societies 2014

Table 1 Comparison of the electrochemical discharge performances of semiconductor–air anodes with various doping types and levels

Anode	Resistivity (Ω cm) and carrier concentration N (cm^{-3})	Operating voltage (V) in 8 h at 10 and 50 μA cm^{-2}	Maximum power density (μW cm^{-2})
n-type Ge	0.007 Ω cm and 8.5 $\times$ 10^{18}	0.79, 0.19	25.7
Undoped Ge	> 45 Ω cm	0.78, 0.49	22.7
p+ Ge	12.5 Ω cm and 2.0 $\times$ 10^{14}	0.68, 0.41	38.9
p++ Ge	0.185 Ω cm and 2.5 $\times$ 10^{16}	0.77, 0.59	208.1
p+++ Ge	0.0145 Ω cm and 1.2 $\times$ 10^{18}	0.75, 0.60	251.7
p-type Si	< 0.005 Ω cm and 1.5 $\times$ 10^{18}	1.23, passivated	37.9
n-type Si	< 0.005 Ω cm and 1.1 $\times$ 10^{18}	1.39, passivated	97.6

n-type Si and p-type Si wafers were also tested to emphasize the inherently favourable kinetics in flat Ge anodes, especially at higher current densities. For example, both n-type Si and p-type Si anodes are already passivated at a discharge current of 50 μA cm^{-2}. As shown in the *J–V* curves in Fig. S2 (ESI†), Si–air cells initially ran at higher operating voltages than Ge–air cells but the voltage quickly reversed to a negative potential, signifying the passivation of the anode. Despite the high doping levels and low resistivities for both n-type Si and p-type Si anodes, the maximum power density is limited by the faster passivation in Si anodes. Although this has a serious implication on the future use of Si anodes in alkaline semiconductor–air batteries, this can be overcome – albeit at a limited degree – by increasing the exposed area of the Si anodes through etching.[17] In contrast, as the carrier concentration in p-type Ge increases, more power is available from the cell: p+, 38.9 μA cm^{-2}; p++, 208.1 μA cm^{-2}; and p+++, 251.7 μA cm^{-2}. The results above prove the excellent discharge kinetics of heavily doped p-type Ge anodes over n-type Ge and doped Si anodes, especially at high current densities. Previous studies have already shown that holes are crucial in the anodic dissolution of semiconductors, such as Ge and Si.[24,25] We believe that the high initial concentration of holes in p-type Ge might be the reason why it exhibits excellent discharge kinetics as an anode over n-type Ge, regardless of whether n-type Ge has a higher Fermi level. Evidently, the discharge performance improved considerably when the carrier concentration in p-type Ge increased.

In order to demonstrate the response of the p-type Ge–air cell (p+++) with abrupt change in current density, a step test was performed from 1 μA cm^{-2}–1.0 mA cm^{-2}. As shown in Fig. 4a, the cell exhibited a very fast response after current cut-off and after a new current density was drawn. This is in agreement with our previous results.[18] In addition, there was a steady voltage drop as the current was increased up to 0.1 mA cm^{-2}, consistent with the results of the *J–V* curve. The OCP notably increases with the discharge time, arising from the increased exposed area and the enhanced anode–electrolyte interface as the discharge process proceeds. This just shows how important the surface area of the anode is to the overall discharge process, allowing the cell to operate at higher voltage and preventing early passivation of the cell.

Fig. 4b displays the big difference in the long-term discharge profiles of n-type Ge and p-type Ge (p+++) anodes. The heavily doped p-type Ge–air cell exhibited a flat voltage profile and
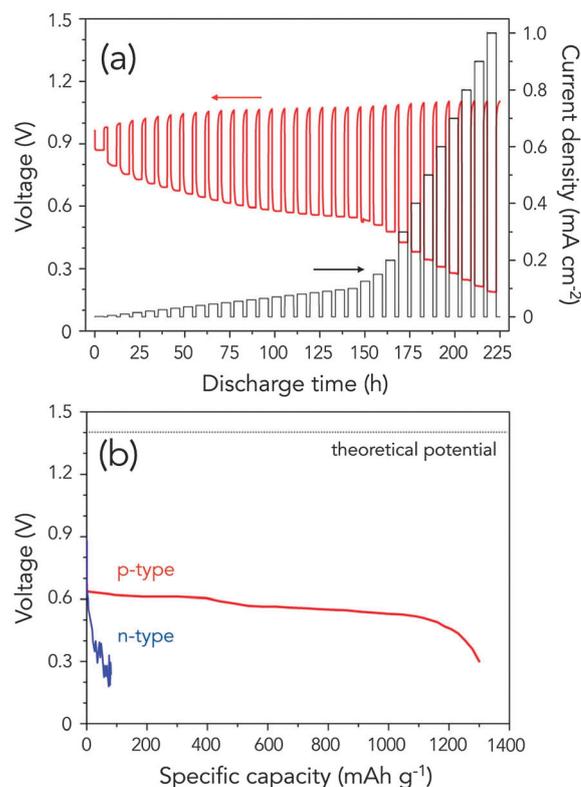

Fig. 4 (a) Dynamic step discharge response of the p-type Ge–air cell (p+++), when operated at increasing current drains. (b) Long-term discharge profiles of n-type Ge and p-type Ge anodes (both heavily doped), showing the huge difference in the electrochemical performance in a Ge–air cell using a 6.0 M gelled KOH electrolyte at a discharge current of 50 μA cm^{-2}.

operated for almost 650 h before the potential gradually dropped. In contrast, n-type Ge operated only for a short time and showed voltage fluctuations, leading to extremely low anode utilization. We surmise that upon n-type Ge oxidation, the concentration of Ge(OH)$_2$ exceeds its solubility quickly, resulting in dehydration and deposition as GeO$_2$ and passivating Ge surface. The poor performance of n-type Ge, however, has been strongly established already from the *J–V* curves above.

In terms of the practical gravimetric capacity, p-type Ge–air cells exhibited a full discharge energy capacity of 1302.5 mA h g$_{Ge}^{-1}$ for the 700 h operation, which is 17 times higher than that of n-type Ge of 77.4 mA h g$_{Ge}^{-1}$ (Fig. 4b). This extremely high anode utilization is close to 88% of the theoretical energy density of 1477.45 mA h g$_{Ge}^{-1}$ based on the anode alone.
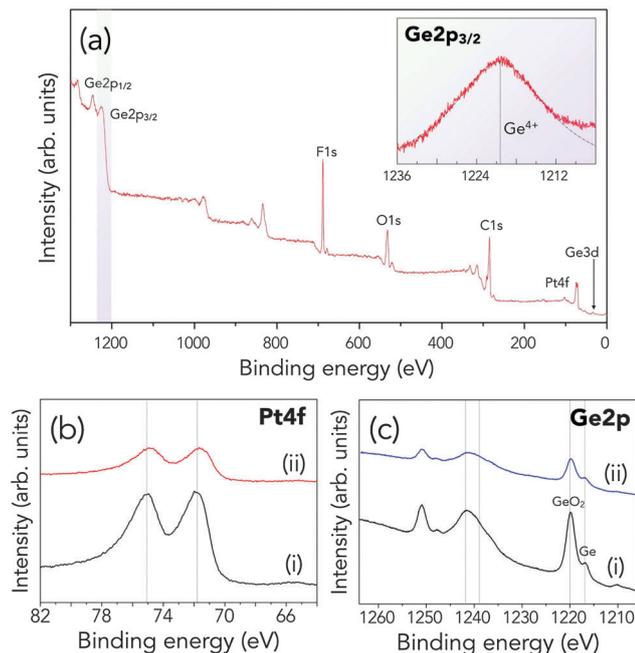
Fig. 5 X-ray photoelectron spectra of the cathode and anode after full discharge for 700 h. (a) XPS survey scan of the Pt/C cathode after discharge, while the inset shows the X-ray photoelectron spectrum of Ge $2p_{3/2}$, fitted with the Ge^{4+} spectrum. (b) Pt 4f XP spectra of Pt/C cathode (i) before and (ii) after full discharge (c) Ge 2p XP spectra of p-type Ge anode (i) before and (ii) after full discharge.

In fact, the Ge–air cell's capacity is two-folds and three-folds higher than that of commercial Zn–air cells (650 mA h g_{Zn}^{-1}, Energizer),[26] and Al–air cells (320 mA h g_{Al}^{-1}, Altek Fuel Group Inc.),[27] respectively. Considering that we are only using a flat p-type Ge anode, this practical energy capacity is even relatively high compared to that in a Zn–air cell using a porous, monolithic, three-dimensional (3D) zinc sponge anodes at 728 mA h g_{Zn}^{-1},[28] a Mg–air cell using a nano-mesoscale structured anode (188 mA h g_{Mg}^{-1}),[29] and an advanced Zn–air cell with high performance hybrid electrocatalysts (570 mA h g_{Zn}^{-1}).[30] Furthermore, p-type Ge–air cell's energy capacity and anode utilization efficiency is notably higher than that of porous Si–air cells with an alkaline electrolyte (1206 mA h g_{Si}^{-1}), which has a capacity corresponding to only 31.6% of Si–air cell's theoretical energy capacity.[17] As summarized in Fig. S3 (ESI†), the long discharge behaviour in p-type Ge–air battery displays key advantages in terms of high practical specific capacity and anode utilization efficiency, which can offset its disadvantages (*e.g.* cost of Ge, lower potential relative to other metal–air chemistries). In order to account for the cell's self-discharge in the long-term operation, we estimated the Ge mass loss due to corrosion from the average corrosion current in p-type Ge (5.02 μA cm^{-2}) and compared it with the actual total mass loss during discharge (see Fig. S4, ESI†). Based on our computations, corrosion mass loss accounts to only 6.4% of the total mass loss during discharge, or less than 1% of the initial mass of Ge anode. Even with an increase in the actual corrosion rate as the surface of Ge is roughened during discharge, the self-discharge

mass loss is still well within the 12% unaccounted Ge, based on the anode utilization efficiency of 88%.

Post discharge characterization on the p-type Ge cell electrodes as shown in Fig. 4b was performed to ascertain if structural and chemical changes occurred after the discharge. As expected, the Ge anode underwent morphological changes, from a flat morphology to a grainy texture (Fig. S5a–d, ESI†), similar to the observed morphology in our previous study.[18] Meanwhile, the Pt/C electrode remained almost the same, especially when examined at higher magnifications in SEM, as seen in Fig. S5e and f (ESI†). Further proof of the unchanged nature of the air cathode is shown by the similar X-ray diffractograms in Fig. S5g (ESI†), prior to and after discharge.

In addition, XPS studies confirmed that some Ge atoms, although it is not yet clear if it's in hydroxide or oxide form, are deposited on the Pt/C electrode (Fig. 5a). In Si–air batteries, formation of reaction products in the cathode during discharge and the conversion of the MnO$_2$ ORR catalyst to inactive MnF$_2$ are considered as major factors in the cell discharge termination.[31,32] However, there seemed to be no adverse effect on the cathode, as there was no shift in the binding energy of Pt 4f as shown in Fig. 5b. If Ge somehow affects the activity of the cathode, especially if non-Pt ORR catalysts are used, this problem could be alleviated by using an anion exchange membrane (AEM) in between the two electrodes. On the other hand, the metallic Ge signal is still visible and the ratio of the metallic Ge and GeO$_2$ in the Ge 2p spectra in Fig. 5c, before and after discharge, even increased slightly. This can mean that the p-type Ge anode might not have been totally passivated and can still continue to discharge. This is consistent with our hypothesis that since the cell is not hermetically sealed, drying out of the electrolyte might have caused the end of discharge. Despite the failure of the cell after 700 h, however, a full discharge capacity of 1302.5 mA h g_{Ge}^{-1} for an anode utilization of 88% represents the highest among semiconductor–air cells already, and even higher than that of conventional metal–air batteries such as Zn–air and Al–air.

3. Conclusions

Our results indicate that the doping type and the degree of doping in semiconductor anodes are crucial in the discharge kinetics in a metal–air battery. We first show that contrary to the conventional wisdom that n-type Ge should show favorable discharge kinetics, p-type Ge behaves extremely better. Heavily doped p-type Ge operates at higher voltage at the high current regime and discharges for a significantly longer time, leading to better utilization and higher energy capacity. It should be emphasized that even if flat semiconductor wafers were used in this study, a very high energy density of 1302.5 mA h g_{Ge}^{-1} for an anode utilization of 88% can be derived from the p-type Ge–air cells. We believe that it is possible to significantly decrease the anodic polarization by downsizing the flat Ge anode to nanoscale Ge. Although a Pt-based ORR catalyst was used in the Ge–air cell operation in this study, it can be replaced

easily with a highly active and inexpensive electrocatalyst based on non-noble metals, as demonstrated in our first report on a Ge–air cell[18] and in our recent studies.[33–35] In addition, increasing the doping degree of semiconductors and enhancing the surface area (*e.g.* 3D structured semiconductor anodes) might potentially lead to better utilization efficiency of the cells and higher operating voltage. While a deeper understanding, especially on the molecular level, of the effect of doping on the discharge kinetics is still needed, the observations here might be extended to Si–air batteries and other semiconductor–air cells. Subsequent studies using careful discharge measurements in the dark (to avoid photocurrents), in addition to density functional theory (DFT) calculations, can help shed light on the nature of the *J–V* behaviour of semiconductor anodes in metal–air cells. In the future, semiconductor–air batteries using SiGe alloys could combine the two extremes of advantages and disadvantages, in terms of cost, discharge kinetics, and operating voltage. SiGe–air cells could provide inherent advantages that are not found individually in Si and Ge. Overall, our results here provide a better understanding on the discharge kinetics of semiconductor anodes in chemical energy conversion devices and might lead to more studies on the effect of doping on semiconductors as they are utilized in other applications (*e.g.* semiconductors in thermoelectrics).

4. Experimental section

4.1 Assembly of semiconductor–air cells

Semiconductor wafer anodes were cut from commercial wafers of different doping types and levels (MTI Corp.). Ge and Si wafers were cleaved to produce 1 cm × 1 cm anodes with 0.785 cm^2 of the flat polished side exposed to the electrolyte *via* an O-ring. All samples were cleaned first using 48 wt% hydrofluoric (HF) solutions (Sigma-Aldrich) to remove the native oxide layer, then afterwards rinsed with deionized (D. I.) water and dried. It should be noted that only flat semiconductor wafers were used in this work. Meanwhile, the air-breathing cathode was constructed by spraying a mixture of 46.7% Pt/C (Tanaka, 1.0 mg cm^{-2}) and Nafion solution (Sigma Aldrich, 10 wt%) on a gas diffusion layer (SGL, 25AA). The gelled KOH electrolyte was prepared by adding sodium carboxymethyl cellulose (CMC, Sigma Aldrich) into the KOH solution (5 wt%) with vigorous stirring and letting the mixture age for three days to ensure complete mixing. Initially, different gelled KOH electrolytes were prepared from 1 wt% to 15 wt% CMC (see Fig. S5, ESI†), but the 5 wt% CMC in KOH showed the best consistency for use as a gelled electrolyte. In order evaluate the electrochemical discharge kinetics of different semiconductor anodes, a single cell – consisting of the Ge anode, gelled KOH electrolyte, Pt/C on GDL cathode, and thin copper (Cu) meshes as current collectors – was assembled. The gelled alkaline electrolyte was injected into the cell through a small hole at the top of the cell. All the cells were assembled and operated under ambient conditions.

4.2 Electrochemical analysis

Potentiodynamic studies were conducted in an electrochemical cell consisting of Pt reference and counter electrodes, n-type Ge or p-type Ge as the working electrode and 6.0 M gelled KOH electrolyte. All the discharge curves were measured in a multi-channel high performance battery tester (Maccor 4300 K, Korea Thermo Tech. Co., Ltd.), using various current densities. Electrochemical impedance spectroscopy was performed with a two-electrode configuration (Zahner Zennium, Zahner Elektrik GmbH & Co.). A 5 mV RMS excitation signal was used with a frequency range of 10 MHz to 1 MHz.

4.3 Post-discharge electrode characterization

Following full discharge of the Ge–air cell, various characterization techniques were used to study the electrodes. For instance, the surface morphology of the pristine and post-discharge electrodes was investigated using a scanning electron microscope (SEM, JEOL JSM 5200), in plain and cross-section views. In addition, X-ray diffraction (XRD, Rigaku D/MAXIIA) study was performed to confirm possible structural changes after the long-term battery discharge. The surface chemical properties of the electrodes were examined by X-ray photoelectron spectroscopy (XPS) with an Mg Kα X-ray source (1253.6 eV) at a base pressure of 2×10^{-9} Torr. After the full discharge, the used electrodes were carefully washed with D. I. water and vacuum-dried fully before the XPS analysis.

Acknowledgements

Notes and references

1 K. F. Blurton and A. F. Sammels, *J. Power Sources*, 1979, **4**, 263–279.
2 D.-W. Park, J. W. Kim, J. K. Lee and J. Lee, *Appl. Chem. Eng.*, 2012, **23**, 359–366.
3 D.-W. Park, J. W. Kim, J. K. Lee and J. Lee, *Appl. Chem. Eng.*, 2012, **23**, 247–252.
4 J.-S. Lee, S. T. Kim, R. Cao, N.-S. Choi, M. Liu, K. T. Lee and J. Cho, *Adv. Energy Mater.*, 2010, **1**, 34–50.
5 B. Scrosati, J. Hassoun and Y.-K. Sun, *Energy Environ. Sci.*, 2011, **4**, 3287–3295.
6 C. Chakkaravarthy, A. K. Abdul Waheed and H. V. K. Udupa, *J. Power Sources*, 1981, **6**, 203–228.
7 Q. Li and N. J. Bjerrum, *J. Power Sources*, 2002, **110**, 1–10.
8 G. Girishkumar, B. McCloskey, A. C. Luntz, S. Swanson and W. Wilcke, *J. Phys. Chem. Lett.*, 2010, **1**, 2193–2203.
9 H. X. Yang, Y. D. Wang, X. P. Ai and C. S. Cha, *Electrochem. Solid-State Lett.*, 2004, **7**, A212–A215.
10 H. Zhang, X. Zhong, J. C. Shaw, L. Liu, Y. Huang and X. Duan, *Energy Environ. Sci.*, 2013, **6**, 2621–2625.

This journal is © the Owner Societies 2014

Phys. Chem. Chem. Phys., 2014, **16**, 22487–22494 | 22493

11 T. N. Lambert, D. J. Davis, S. J. Limmer, M. R. Hibbs and J. M. Lavin, *Chem. Commun.*, 2011, **47**, 9597–9599.

12 K. Harting, U. Kunz and T. Turek, *Z. Phys. Chem.*, 2012, **226**, 151–166.

13 X. G. Zhang, *J. Power Sources*, 2006, **163**, 591–597.

14 G. Cohn, D. Starosvetsky, R. Hagiwara, D. D. Macdonald and Y. Ein-Eli, *Electrochem. Commun.*, 2009, **11**, 1916–1918.

15 G. Cohn and Y. Ein-Eli, *J. Power Sources*, 2010, **195**, 4963–4970.

16 G. Cohn, A. Altberg, D. D. Macdonald and Y. Ein-Eli, *Electrochim. Acta*, 2011, **58**, 161–164.

17 X. Zhong, H. Zhang, Y. Liu, J. Bai, L. Liao, Y. Huang and X. Duan, *ChemSusChem*, 2012, **5**, 177–180.

18 J. D. Ocon, J. W. Kim, S. Uhm, B. S. Mun and J. Lee, *Phys. Chem. Chem. Phys.*, 2013, **15**, 6333–6338.

19 J. D. Ocon, J. K. Lee and J. Lee, *Appl. Chem. Eng.*, 2014, **25**, 1–13.

20 A. A. Mohamad, *J. Power Sources*, 2006, **159**, 752–757.

21 R. O'Hayre, S.-W. Cha, W. Colella and F. B. Prinz, *Fuel Cell Fundamentals*, John Wiley & Sons, New York, 1st edn, 2006.

22 R. W. Schutz, *Corrosion: Materials*, ASM Handbook, SM International, Material Park, vol. 13B, 2005.

23 D. B. Cuttris, *Bell Syst. Tech. J.*, 1961, **40**, 509–523.

24 V. A. Myamlin and Y. V. Pleskov, *Russ. Chem. Rev.*, 1963, **32**, 208–223.

25 C. A. Koval and J. N. Howard, *Chem. Rev.*, 1992, **92**, 411–433.

26 http://data.energizer.com/PDFs/675.pdf.

27 http://www.altekfuel.com/userfiles/File/SDS_APS100_12-24_V-04.pdf.

28 J. F. Parker, C. N. Chervin, E. S. Nelson, D. R. Rolison and J. W. Long, *Energy Environ. Sci.*, 2014, **6**, 1117–1124.

29 W. Li, C. Li, C. Zhou, H. Ma and J. Chen, *Angew. Chem., Int. Ed.*, 2006, **45**, 6009–6012.

30 Y. Li, M. Gong, Y. Liang, J. Feng, J.-E. Kim, H. Wang, G. Hong, B. Zhang and H. Dai, *Nat. Commun*, 2013, **4**, 1805.

31 G. Cohn, D. D. Macdonald and Y. Ein-Eli, *ChemSusChem*, 2011, **4**, 1124–1129.

32 P. Jakes, G. Cohn, Y. Ein-Eli, F. Scheiba, H. Ehrenberg and R. Eichel, *ChemSusChem*, 2012, **5**, 2278–2285.

33 B. Jeong, D. Shin, H. Jeon, J. D. Ocon, B. S. Mun, J. Baik, H.-J. Shin and J. Lee, *ChemSusChem*, 2014, **5**, 1289–1294.

34 D. Shin, B. Jeong, B. S. Mun, H. Jeon, H.-J. Shin, J. Baik and J. Lee, *J. Phys. Chem. C*, 2013, **4**, 11619–11624.

35 D. Phihusut, J. D. Ocon, B. Jeong, J. W. Kim, J. K. Lee and J. Lee, *Electrochim. Acta*, DOI: 10.1016/j.electacta.2014.05.050, in press.

22494 | *Phys. Chem. Chem. Phys.*, 2014, **16**, 22487–22494

This journal is © the Owner Societies 2014